Free volume of an oligomeric epoxy resin and its relation to structural relaxation: Evidence from positron lifetime and pressure-volume-temperature experiments

Günter Dlubek*
ITA Institut für Innovative Technologien, Köthen/Halle, Wiesenring 4, D-06120 Lieskau (Halle/S.), Germany

Jürgen Pointeck
Leibniz-Institut für Polymerforschung Dresden e.V., Hohe Strasse 6, D-01069 Dresden, Germany

Muhamad Qasim Shaikh, E. M. Hassan, and Reinhard Krause-Rehberg
Fachbereich Physik, Martin-Luther-Universität Halle-Wittenberg, D-06099 Halle/S., Germany
(Received 22 September 2006; published 22 February 2007)

From positron annihilation lifetime spectroscopy analyzed with the new routine LT9.0 and pressure-volume-temperature experiments analyzed employing the equation of state (EOS) Simha-Somcynsky lattice-hole theory (SS EOS) the microstructure of the free volume and its temperature dependence of an oligomeric epoxy resin (ER6, $M_n \approx 1750$ g/mol, $T_g = 332$ K) of diglycidyl ether of bisphenol-*A* (DGEBA) have been examined and characterized by the hole free-volume fraction h, the specific free and occupied volumes $V_f = hV$ and $V_{\mathrm{occ}} = (1-h)V$, and the size distribution (mean, $\langle \nu_h \rangle$, and mean dispersion, σ_h) and the mean density $N_h' = V_f / \langle \nu_h \rangle$, of subnanometer-size holes. The results are compared with those from a previous work [G. Dlubek *et al.*, Phys. Rev. E **73**, 031803 (2006)] on a monomeric liquid of the same resin (ER1, $M_n \approx 380$ g/mol, $T_g = 255$ K). In the glassy state ER6 shows the same hole sizes as ER1 but a higher V_f and N_h'. In the liquid V_f, $\langle \nu_h \rangle$, dV_f/dT, and dV_f/dP are smaller for ER6. The reported dielectric α relaxation time τ shows certain deviations from the free-volume model which are larger for ER6 than for ER1. This behavior correlates with the SS EOS, which shows that the unit of the SS lattice is more heavy and bulky and therefore the chain is less flexible for ER6 than for ER1. The free-volume fraction h in the liquid can be described by the Schottky equation $h \propto \exp(-H_h/k_B T)$, where $H_h = 7.8$–6.4 kJ/mol is the vacancy formation enthalpy, which opens a different way for the extrapolation of the equilibrium part of the free volume. The extrapolated h decreases gradually below T_g and becomes zero only when 0 K is reached. This behavior means that no singularity would appear in the relaxation time at temperatures above 0 K. To quantify the degree to which volume and thermal energy govern the structural dynamics, the ratio of the activation enthalpies $E_i = R[(d \ln \tau / dT^{-1})]_i$, at constant volume V and constant pressure P (E_V/E_P), is frequently determined. We present arguments for necessity to substitute E_V by E_{Vf}, the activation enthalpy at constant (hole) free volume, and show that E_{Vf}/E_P changes as expected: it increases with increasing free volume, i.e., with increasing temperature, decreasing pressure, and decreasing molecular weight. E_{Vf}/E_P exhibits smaller values than E_V/E_P, which leads to the general inference that the free volume plays a larger role in dynamics than concluded from E_V/E_P. The same conclusion is obtained when scaling τ to $T^{-1}V_f^{-\gamma}$ instead of to $T^{-1}V^{-\gamma}$, where both γ's are material constants.

DOI: 10.1103/PhysRevE.75.021802 PACS number(s): 61.41.+e, 64.70.Pf, 65.40.De, 78.70.Bj

I. INTRODUCTION

In a recently published work [1] we have studied the microstructure of the free volume and its temperature dependence in a low molecular, monomeric resin of diglycidyl ether of bisphenol-*A* (DGEBA) using positron annihilation lifetime spectroscopy (PALS) and pressure-volume-temperature (PVT) experiments. The PVT data were analyzed employing the equation of state (EOS) of the Simha-Somcynsky lattice-hole theory (SS EOS) [2–4]. This theory describes a liquid as a periodic lattice of cells of equal size each having $z = 12$ nearest neighbors. The disorder is modeled by assuming a statistical mixture of occupied and unoccupied cells. From this analysis the fraction of empty cells (holes or vacancies) h is estimated. The vacancies in the SS lattice constitute the hole free volume $V_f = V_{fh} = hV$. The occupied volume $V_{\mathrm{occ}} = (1-h)V$ contains the van der Waals volume V_W [5], and an empty space, which may be denoted as interstitial free volume V_{fi}. That means that the free volume in the SS theory is an excess free volume, which has a similar meaning as the free volume in the definitions of Doolittle [6] or Bondi [7]. Free volume defined in a comparable way also appears in the Cohen-Turnbull free-volume theory, derived on the basis of statistical mechanics [8].

The PALS method uses the positronium (Ps), a light quantum-mechanical particle with the mass of two electrons, and the size of a hydrogen atom, as a probe to measure the size of subnanometric holes in amorphous solids or liquids [9,10]. Ps is formed in molecular matter and (*Anderson*) localized at local free volumes (denoted as holes). The long-lived *ortho* state of Ps (*o*-Ps) is very sensitive to the hole size. Its lifetime decreases from 142 ns in infinite large holes (self-annihilation in a vacuum) to the low ns range in subnanometer-size holes and mirrors the hole size at the mo-

*Author to whom correspondence should be addressed. Electronic address: gdlubek@aol.com

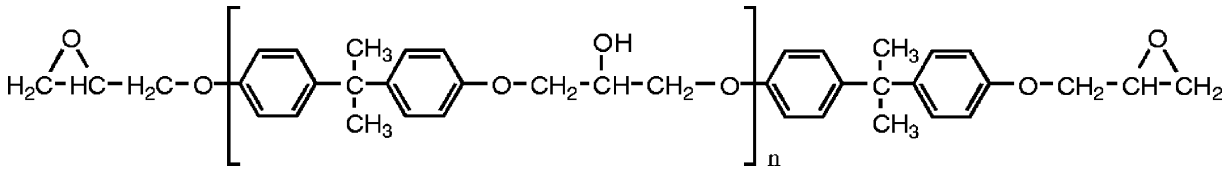

FIG. 1. The chemical structure of DGEBA. $n \approx 0.18$ for ER1 and $n \approx 5$ for ER6.

ment of annihilation. The decrease in lifetime occurs since *o*-Ps may annihilate with an electron other than its bound partner, and with opposite spin, during a collision with a molecule in the hole wall (pickoff annihilation) [9,10].

Recently, it was shown that the holes detected by *o*-Ps can be considered as multiplets of the vacancies described by the SS EOS, which appear due to statistical reasons as a consequence of the large number of vacancies [11–15]. Both methods, PALS and PVT (SS), are therefore complementary and deliver a complete description of the structure of the free volume: the hole size distribution usually characterized by its mean and mean dispersion, the number density of holes, and the fraction and the specific value of the hole free volume [12–18].

The aim of our study is to characterize the free volume in an oligomeric epoxy resin of DGEBA in a pure, uncured state as completely as possible and to use this to test the validity of the Cohen-Turnbull free-volume theory [8], to discover possible deviations from the expected behavior, and to discuss physical reasons for these deviations. A very detailed study of the dynamics of this material employing dielectric spectroscopy, dynamic light scattering-photon correlation spectroscopy, and mechanical spectroscopy was published recently by Paluch *et al.* [19].

An important part of our work is to systematically study the differences in the free-volume structure of the oligomeric DGEBA to the properties of the monomeric liquid of the same resin, which we have published recently [1]. Therefore, we will not repeat all the details of the theory and data analysis, but instead of, make reference to the previous work. Figure 1 shows the chemical formula of DGEBA. The molecules of the sample studied in the current work have a mean length of $n \approx 5$ while the former sample [1] has $n \approx 0.18$. For shortness we denote both DGEBA resins as ER6 and ER1. The important point for our interest is that the properties of the resins differ distinctly due to their different molecular mass without a change in the chemistry of the material. For example, ER6 has a caloric glass transition at 332 K [19,20] while for ER1 a value of 255 K [21] has been determined.

A further important aspect of this study, which goes beyond our first work, is the discussion of the central question of glass formation and what governs the kinetic arrest of the quenched liquid—cooling reduces the thermal energy that molecules need to surmount local potential barriers, while the accompanying volume contraction promotes molecular crowding and congestion. Following the literature [22–27] we attempt to quantify the degree to which thermal energy and volume govern the structural relaxation of the material by determining the ratio of the activation enthalpies of α relaxation at constant volume and at constant pressure, E_V/E_P. We criticize this procedure and present arguments that it is physically more reasonable to use E_{Vf}, the activation enthalpy at constant hole free volume, instead of E_V. Our estimation gives lower values for E_{Vf}/E_P, which shows that the free volume plays a larger role in structural dynamics than concluded usually from the ratio E_V/E_P. We show also that E_{Vf}/E_P increases with increasing temperature, decreasing pressure, and decreasing molecular weight, which is in qualitative agreement with the expectations. That is not always true for the ratio E_V/E_P [26,27]. Reasons for the unexpected behavior of E_V/E_P are discussed.

II. EXPERIMENT

The material used in this study was a DGEBA from Aldrich. This oligomer is synthesized by the reaction of bisphenol-*A* with epichlorohydrin. Its number-averaged molecular weight M_n is about 1750 g/mol, corresponding to $n \approx 5$ in Fig. 1. It is the same material as used in the dynamic study by Paluch *et al.* [19].

Standard PVT experiments were carried out by means of a fully automated GNOMIX high-pressure dilatometer [28] having a relative and an absolute accuracy of 0.0002 cm^3/g and 0.002 cm^3/g, respectively. The densities of the samples at room temperature were determined by means of an Ultrapycnometer 1000 (Quantachrome) with an accuracy of 0.03%.

The PALS measurements were done using a fast-fast coincidence system [9,10] with a time resolution of 266 ps (FWHM, ^{22}Na source) and an analyzer channel width of 25.5 ps. Each measurement lasted six hours leading to a lifetime spectrum of $\sim 5 \times 10^6$ coincidence. All other parameters of the experiments are the same as in our previous work [1].

III. RESULTS AND DISCUSSION

A. Total, occupied, and free volume

Figure 2 shows a series of volume V isobars with the pressure P as the parameter, the fits of the SS EOS [Eq. (5) in Ref. [1]] to the data from above $T_g(P)$, and the calculated occupied volume $V_{occ}=(1-h)V$. The behavior of the specific hole free volume $V_f=hV$ is shown in Fig. 3. The SS EOS expresses pressure, volume, and temperature in reduced units. Their scaling parameters P^*, V^*, and T^* were estimated from a consecutive evaluation procedure. It is common to estimate the fractional hole free volume h from the specific volume above and below $T_g(P)$ [via Eq. (4) in Ref. [1]] using P^*, V^*, and T^* determined for the melt. The h values of the glass are considered to be sufficiently good approximations for conditions not too far from equilibrium [3].

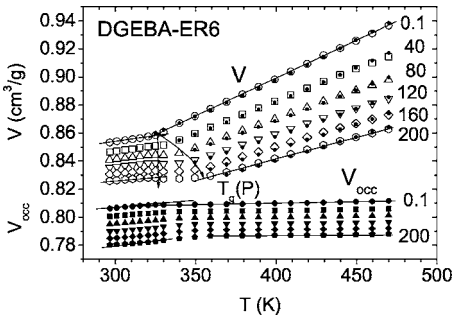

FIG. 2. Specific total, V (empty symbols), and occupied, $V_{occ}=(1-h)V$ (filled symbols), volume of DGEBA-ER6 as a function of temperature T and as a selection of isobars (in MPa). The dots within the open symbols represent the fits of the SS EOS to the experiment.

The scaling parameters and other characteristic values of the volume of ER6 are shown in Table I together with the data for ER1. M_0 is the molecular weight of a SS MER, which can be calculated from $M_0=RT^*/(3P^*V^*)$ (R is the gas constant). The volume of a SS cell follows from $\nu_{SS}=M_0V_{occ}/N_A$ (N_A—Avogadro's constant). The coefficients of thermal expansion and the compressibilities displayed in Table I have the usual meaning [1]. The fractional parameters marked by "*" are defined by $\alpha_i^*=(1/V)(dV_i/dT)|_P$ and $\kappa_i^*=-(1/V)(dV_i/dP)|_T$ (i=occ, f). As found in various previous works [12,14] $\alpha_{occ,g}^*\approx 0.5\alpha_g\approx 1\times10^{-4}$ K^{-1} ($T<T_g$) and $\alpha_{occ,r}^*\approx\alpha_{occ,r}\approx 0.2\times10^{-4}$ K^{-1} ($T>T_g$: g denotes the glass and r the rubber) while $\kappa_{occ,g}^*\approx\kappa_{occ,r}\approx 1.5\times10^{-4}$ MPa^{-1}. This means that above T_g the occupied volume shows a very weak expansion but it is remarkably compressible. The consequence is that the hole (or excess) free volume $V_f=V-V_{occ}$ is not the same for the same total volume $V(P,T)$ but different P, T pairs. We remark here that this is not true for total free volume $V_{ft}=V-V_W$. It is the same for the same total volume $V(P,T)$ but different P, T pairs under the assumption that the van der Waals volume V_W does not depend on P and T. The coefficient of thermal expansion of the free volume α_f is one order of magnitude larger than the one of the total volume. The same is true for the compressibility $\kappa_{f,r}$ above T_g.

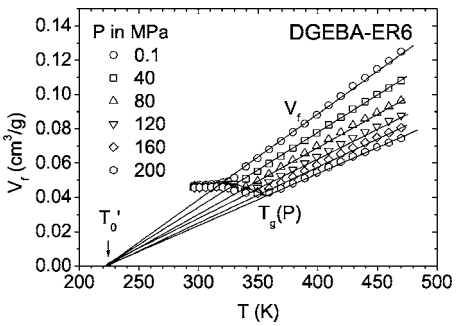

FIG. 3. The specific hole free volume $V_f=hV$ of DGEBA-ER6 as a function of temperature T and as a selection of isobars. The solid lines are due to fits of Eq. (1) to the data from above $T_g(P)$. T_0' is the temperature where the linearly extrapolated hole free volume vanishes.

TABLE I. Results from the analysis of PVT experiments (for an explanation of the symbols see the text).

Quantity	Uncertainty	ER1	ER6
M_n (g/mol)		~380	~1750
n (in Fig. 1)		~0.18	~5.4
T_g (DSC, K)[i]	±1	255	332
T_g (PVT, K)	±2		325
T_0' (K)	±5	209	223
V (cm³/g)[a]	±0.002	0.8572	0.8533
V_W (cm³/g)[g]		0.587	0.587
V_{occ} (cm³/g)[a]	±0.003	0.8046	0.8062
V_f (cm³/g)[a]	±0.003	0.0526	0.0471
E_{f0} (10^{-4} cm³ g^{-1} K^{-1})	±0.04	6.034	5.04
a (10^{-3} MPa^{-1})	±0.005	3.168	3.240
h[a]	±0.003	0.0613	0.0557
$h_g=h(T_g)$	±0.003	0.0334	0.0576
α_g (10^{-4} K^{-1})	±0.05		2.15[c]
α_r (10^{-4} K^{-1})	±0.05	6.79[b]	6.263[d]
$\alpha_{occ,g}$ (10^{-4} K^{-1})	±0.05		1.222[c]
$\alpha_{occ,g}^*$ (10^{-4} K^{-1})	±0.05		1.115[c]
$\alpha_{occ,r}$ (10^{-4} K^{-1})	±0.05	0.28[b]	0.249[d]
$\alpha_{occ,r}^*$ (10^{-4} K^{-1})	±0.05	0.26[b]	0.234[d]
$\alpha_{f,g}$ (10^{-4} K^{-1})	±1		17.9[c]
$\alpha_{f,g}^*$ (10^{-4} K^{-1})	±0.05		1.034[c]
$\alpha_{f,r}$ (10^{-4} K^{-1})	±1	106.5[b]	104.7[d]
$\alpha_{f,r}^*$ (10^{-4} K^{-1})	±0.05	6.51[b]	6.029[d]
κ_g (10^{-4} MPa^{-1})	±0.05		1.8[e]
κ_r (10^{-4} MPa^{-1})	±0.05	3.32[b]	3.82[f]
$\kappa_{occ,g}$ (10^{-4} MPa^{-1})	±0.1		1.62[e]
$\kappa_{occ,g}^*$ (10^{-4} MPa^{-1})	±0.1		1.53[e]
$\kappa_{occ,r}$ (10^{-4} MPa^{-1})	±0.1	1.36[b]	1.44[f]
$\kappa_{occ,r}^*$ (10^{-4} MPa^{-1})	±0.1	1.28[b]	1.32[f]
$\kappa_{f,g}$ (10^{-4} MPa^{-1})	±1		4.95[e]
$\kappa_{f,g}^*$ (10^{-4} MPa^{-1})	±0.1		0.274[e]
$\kappa_{f,r}$ (10^{-4} MPa^{-1})	±1	33.3[b]	32.3[f]
$\kappa_{f,r}^*$ (10^{-4} MPa^{-1})	±0.1	2.043[b]	2.46[f]
T^* (K)	±20	9941	11176
V^* (cm³/g)	±0.003	0.8432	0.8474
P^* (MPa)	±20	1190	1150
M_0 (g/mol)	±0.3	28.7	33.5
ν_{SS} (Å³)[a]	±0.5	38.3	45.0
H_h (kJ/mol)	±0.1	6.88[a]/5.91[h]	7.82[d]/6.42[h]
δ (MPa$^{1/2}$)	±0.5	27.9[a]/24.8[h]	27.6[d]/25.3[h]

[a]At 300 K.
[b]At $T=T_g+42$ K=297 K (ER1).
[c]At $T\to T_g=325$ K, $T<T_g$.
[d]At $T\to T_g=325$ K, $T>T_g$.
[e]At $T=T_g-24$ K=301 K.
[f]At $T=T_g+34$ K=359 K (all for ER6).
[g]From Reference [5].
[h]At 470 K.
[i]From differential scanning calorimetry (DSC), References [19–21].

As in our previous work [1] we have analyzed the specific free volume above T_g in terms of the equation

$$V_f(T,P) = [E_{f0}/(1+aP)](T - T_0'), \quad (1)$$

where $E_{f0} = (dV_f/dT)|_{P=0}$ is the specific thermal expansivity for zero pressure and T_0' is the temperature where the extrapolated free volume goes to zero. In unconstrained fits T_0' varied unsystematically between 218 and 228 K. In the final fits we fixed T_0' to its average of 223 K and got the values of E_{f0} and a shown in Table I.

The vacancies of the SS lattice are by definition *Schottky* defects. We may therefore attempt to describe their concentration by the Schottky equation [29]

$$h = A \exp(-H_h/k_B T), \quad (2)$$

where H_h is the hole formation enthalpy, A is a preexponential factor, and k_B is the Boltzmann constant. A linear fit to the data of ER6 in an Arrhenius plot delivers $A=0.80$ and $H_h=7.03$ kJ/mol ($r^2=0.999\,36$, not shown). This value is not far from $H_h \approx 3RT_g$ estimated by Perez from caloric data [30]. A fit of a quadratic function to the Arrhenius plot gives a slightly better fit ($r^2=0.999\,87$) and shows a slight change in $H_h = -k_B\,[\partial \ln h/\partial(1/T)]_P$ from 7.82 kJ/mol at 330 K to 6.42 kJ/mol at 470 K. These values correspond to 0.38–0.34 of the cohesive energy E_c of a SS MER calculated from the SS EOS to be 20.8 and 19.1 kJ/mol, respectively, at these temperatures. The ratio H_h/E_c has a reasonable value since a MER in a surface plane has only eight nearest neighbors, which means that the vacancy formation in the closed packed structure is connected with the destruction of $(12-8)/12 = 1/3$ of the total number of bonds. It is interesting that H_h mirrors the temperature dependency of the cohesive energy. We will come back to these results later. We remark at this point that the solution parameter δ may be calculated from the cohesive energy density (*CED*) via $\delta = \mathrm{CED}^{1/2}$ [4]. Table I shows the results for both epoxy resins for two different temperatures.

The comparison of ER6 with ER1 shows that ER6 has the higher T_g, T_0', and above T_g a lower total V, and free, V_f, volume (at the same temperature). The occupied volume V_{occ} and its expansivity and compressibility are almost the same. The same is true for the coefficient of thermal expansion and compressibility of free volume above T_g, $\alpha_{f,r}$, and $\kappa_{f,r}$. In this comparison, however, the different temperatures and values of free volume V_f have to be considered. At ambient pressure the specific thermal expansivity of the free volume $E_{f0} = dV_f/dT$ is smaller for ER6 (5.04×10^{-4} cm^3 g^{-1} K^{-1}) than for ER1 (6.03×10^{-4} cm^3 g^{-1} K^{-1}). The same is valid for the compressibility parameter $dV_f/dP = \kappa_f V_f$, which has at 350 K a value of 2.12×10^{-4} cm^3 g^{-1} MPa^{-1} for ER6 and 2.53×10^{-4} cm^3 g^{-1} MPa^{-1} for ER1. This behavior correlates with the parameter T^*, M_0, ν_{ss}, and H_h, which show that the MER of the SS lattice is more heavy and bulky for ER6 than for ER1.

B. Size and number density of holes

As in our previous work [1] we analyzed the positron lifetime spectra employing the routine LIFETIME, version 9.0 [31], and assuming three exponential-like lifetime components, which come from the annihilation of *p*-Ps (*para*-positronium, mean lifetime τ_1), positrons (e^+, τ_2), and *o*-Ps (τ_3; $\tau_1 < \tau_2 < \tau_3$) [9,10]. LT9.0 assumes that the functions $\alpha_i(\lambda)\lambda$ follow a logarithmic Gaussian function where $\alpha_i(\lambda)$ is the distribution function of the annihilation rate λ ($\lambda = 1/\tau$) of each decay channel i. We assumed that the *p*-Ps lifetime appears discrete ($\sigma_1 = 0$), while the positron and *o*-Ps lifetimes were allowed to show a distribution ($\sigma_2, \sigma_3 > 0$) [1].

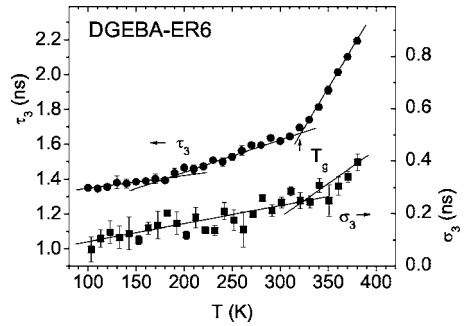

FIG. 4. Mean τ_3 and mean dispersion σ_3 of the *o*-Ps lifetime in DGEBA-ER6. The lines through the data points are a visual aid. The arrow shows the glass transition.

Free-floating parameters of the fit were the time zero t_0 of the spectrum, the mean lifetimes τ_1, τ_2, τ_3, the mean dispersions σ_2 and σ_3, and the relative intensity of *o*-Ps annihilation, I_3. The two other intensities were constrained to $I_2 = 1 - (I_1 + I_3)$ and $I_1/I_3 = 1/3$, where $P = I_1 + I_3$ is the Ps yield and I_1/I_3 mirrors the theoretical ratio of the *p*-Ps and *o*-Ps formation [9,10]. A least-squares fit of the model function to the experimental spectrum, with an added background B and a correction with respect to the annihilation events in the source, all convoluted with the resolution function (a sum of two Gaussians), delivers the mentioned parameters of the lifetime spectrum.

Figure 4 shows the temperature dependence of the mean τ_3 and mean dispersion σ_3 of the lifetime distribution of *o*-Ps. τ_3 varies between 1.35 ns at 100 K and 2.20(±0.02) ns at 380 K, and σ_3 between 0.10 ns and 0.40(±0.03) ns. τ_3 mirrors the mean size of free-volume holes in which *o*-Ps annihilates, and σ_3 the width of the hole size (and shape) distribution. Both values show a distinct increase in their slopes at 321 K, a temperature which is interpreted as T_g. τ_3 shows an additional, weaker change in its gradient at 180 K.

The intensity I_3 of the *o*-Ps component of ER6 increases linearly from 25.5% at 100 K to 30.0(±0.2)% at 380 K (not shown). The mean positron (e^+) lifetime τ_2 (not shown) exhibits a similar behavior to τ_3. τ_2 increases from 0.305 ns to 0.325(±0.003) ns and the mean dispersion σ_2 from 0.06 ns at 100 K to 0.10(±0.02) ns at 350 K. The *p*-Ps lifetime $\tau_1$fluctuates between 0.100 and 0.125 ns with a mean of 0.115(±0.003) ns.

In the following section we analyze the behavior of the hole volume of ER6 and correlate these data with those from PVT studies. Based on the semiempirical Tao-Eldrup (standard) model [32,33] the *o*-Ps pickoff annihilation rate λ_{po}, the inverse of the *o*-Ps lifetime $\tau_{\mathrm{po}} = \tau_3$, is related to the hole (assumed spherical) radius (r_h) via

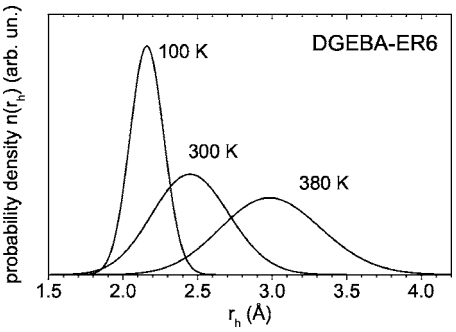

FIG. 5. Hole radius distribution $n(r_h)=-\alpha_3(\lambda)d\lambda/dr_h$ for three selected temperatures of DGEBA-ER6. The curves are normalized to the free-volume fraction of $\int \nu_h g_n(\nu_h)d\nu_h=1$.

$$\lambda_{\mathrm{po}} = 1/\tau_{\mathrm{po}} = 2ns^{-1}\left[1 - \frac{r_h}{r_h+\delta r} + \frac{1}{2\pi}\sin\left(\frac{2\pi r_h}{r_h+\delta r}\right)\right], \quad (3)$$

where δr (=1.66 Å [33,34]) describes the penetration of the Ps wave function into the hole walls. The mean hole volume is usually calculated from $\nu_h(\tau_3)=(4/3)\pi r_h^3(\tau_3)$. Since λ_{po} follows a distribution, we have estimated, as in our previous work [1], the mean hole volume as the mass center of the hole size distribution. The radius distribution $n(r_h)$ can be calculated from $n(r_h)=-\alpha_3(\lambda)d\lambda/dr_h$ [35,36], where $\alpha_3(\lambda)$ is the *o*-Ps annihilation rate distribution calculated from the parameters of the LT analysis. The hole size distribution follows from $g(\nu_h)=n(r_h)/4\pi r_h^2$ and is considered as a volume-weighted function. The number-weighted hole size distribution follows then from $g_n(\nu_h)=g(\nu_h)/\nu_h$. The mean and the variance of $g_n(\nu_h)$,$\langle\nu_h\rangle$ and σ_h^2, were calculated numerically as first and second moments of this distribution.

Figure 5 shows, as an example, plots of the hole radius distribution $n(r_h)$ calculated from $\alpha_3(\lambda)$ for 100, 300, and 380 K. The function $n(r_h)$ can be well approximated by a Gaussian. Gaussian-type hole size distributions were analyzed for holes in various simulated polymer structures [37–39]. The center and width of the Gaussian distribution of ER6 shift with increasing temperature to higher values, particularly above T_g. At 100 K the hole size distribution extends from 1.88 to 2.45 Å (measured at a height of 0.05 of the maximum of the distribution) with the maximum at 1.97 Å, and at 380 K from 2.2 to 3.8 Å with a maximum at 2.98 Å.

The mean hole volume $\langle\nu_h\rangle$ and the corresponding mean hole volume dispersion σ_h for the two resins are plotted in Fig. 6. Both parameters show the expected behavior with the glass transition at T_g=321 K for ER6 and 260 K for ER1. At T_g the thermal expansivity $e_h=d\langle\nu_h\rangle/dT$, and the coefficient of thermal expansion $\alpha_h=e_h/\langle\nu_{hg}\rangle$ ($\langle\nu_{hg}\rangle=\langle\nu_h(T_g)\rangle$) of free volume holes change abruptly from the value for the glass to the rubber. The slightly larger values of $\langle\nu_h\rangle$ for ER6 at low temperature in comparison with ER1 show that the molecules in the oligomer are packed less densely than in the monomer. Secondary relaxation processes [21,55] usually do not exhibit a volumetric activity. The parameters of the hole volume expansion are shown in Table II. The detailed comparison with the data for ER1 will be done later.

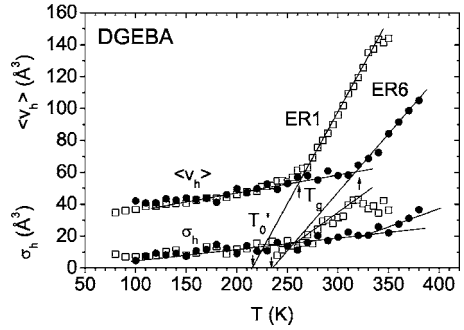

FIG. 6. The mean hole volume $\langle\nu_h\rangle$, and the mean hole volume dispersion σ_h, calculated from the number-weighted hole volume distribution $g_n(\nu_h)$ as a function of the temperature T for DGEBA-ER6 (filled symbols) and DGEBA-ER1 (empty symbols). The lines are linear least-squares fits to the data from above and below T_g. T_g and T_0' indicate the volumetric glass transition and the temperature where the hole volume linearly extrapolated from $T>T_g$ goes to zero.

As we have shown recently [12–15], the knowledge of the mean dispersion of the hole volume σ_h allows one to estimate the mean square fluctuation of the free volume $\langle\delta V_f^2\rangle$ and from this the mean volume $\langle V_{SV}\rangle$ of the smallest representative free fluctuation subsystem related to structural relaxation. The physics concluded from the temperature dependency of $\langle V_{SV}\rangle$ were discussed in detail in Ref. [1] for ER1 and more generally in Ref. [15]. The conclusions for ER6 are quite similar, therefore we go on without presenting this analysis.

For a complete characterization of the free volume we still need the density of holes. This can be obtained from a comparison of PALS with PVT data. The mean number of holes per mass unit N_h' is usually determined from one of the relations [40]

$$V_f = hV = N_h'\langle\nu_h\rangle, \quad (4)$$

$$V = V_{\mathrm{occ}} + N_h'\langle\nu_h\rangle. \quad (5)$$

TABLE II. Results from the analysis of the PALS experiments. (For an explanation of symbols see the text.)

Quantity	Uncertainty	ER1	ER6
T_g (K)	±3	260	321
T_0' (K)	±10	214	233
$\langle\nu_{hg}\rangle$ (Å^3)	±3	52	60
e_{hg} (Å^3/K)[b]	±0.02	0.092	0.131
e_{hr} (Å^3/K)[c]	±0.03	1.13	0.717
$\alpha_{hg}(10^{-3}$ K$^{-1})$[b]	±0.2	1.78	2.18
α_{hr} (10^{-3} K^{-1})[c]	±1	21.9	12.0
N_h' (10^{21} g^{-1})	±0.02	0.56	0.75
N_h (nm^{-3})[a]	±0.02	0.65	0.88

[a]At 300 K.
[b]At $T\to T_g$, $T<T_g$.
[c]At $T\to T_g$, $T>T_g$.

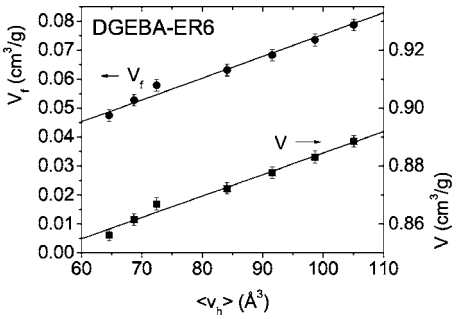

FIG. 7. The specific free, $V_f(T)$, and total, $V(T)$, volume plotted versus the mean hole volume $\langle \nu_h(T) \rangle$ for DGEBA-ER6. The slopes of both plots determine the specific hole density N_h'.

The plot V_f vs $\langle \nu_h \rangle$ of the data from above T_g displayed in Fig. 7 shows a linear dependency from which a constant slope of $dV_f/d\langle \nu_h \rangle = 0.72(\pm 0.04) \times 10^{21}$ g^{-1} and an intercept with the y axis of $V_{f0} = 0.0032(\pm 0.003)$ cm^3/g can be estimated. A plot of V vs $\langle \nu_h \rangle$ delivers similar results, $dV/d\langle \nu_h \rangle = 0.74(\pm 0.04) \times 10^{21}$ g^{-1} and $V_{\rm occ} + V_{f0} = 0.8106(\pm 0.003)$ cm^3/g. A linear fit to the V_f vs $\langle \nu_h \rangle$ plot constrained to pass zero gives for the specific hole number $N_h' = dV_f/d\langle \nu_h \rangle = 0.75(\pm 0.02) \times 10^{21}$ g^{-1}. This corresponds to a volume related hole density of $N_h = N_h' \rho = 0.88(\pm 0.02)$ nm^{-3} at 300 K ($\rho = 1/V$).

The comparison of ER6 with ER1 shows that both materials exhibit almost the same hole sizes in the glassy state. Above T_g ER6 has the lower mean hole volume $\langle \nu_h \rangle$ due to its higher T_g and a lower expansivity. This behavior agrees with the specific total and free volume. Below T_g, however, the specific free volume V_f is larger for ER6 than for ER1. Figure 8 plots V_f from PVT and PALS experiments for ER6 and ER1. (We shall discuss the values V_f^m and the inset in Fig. 8.) The higher V_f in ER6 leads to the higher number density of holes calculated from $N_h' = V_f/\langle \nu_h \rangle$. We attempt to explain this unexpected but interesting result in the following section.

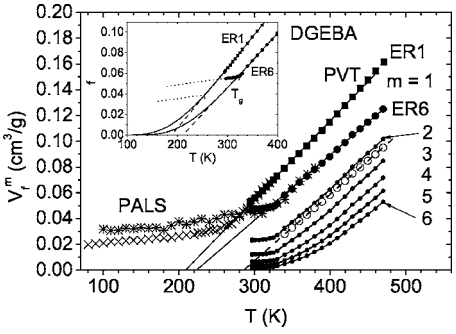

FIG. 8. Specific free volume at ambient pressure $V_f = V_f^1$ for DGEBA-ER6 and DGEBA-ER1 from PVT ($V_f = hV$, filled symbols) and PALS ($V_f = N_h' \langle \nu_h \rangle$, stars and crosses) experiments. For ER6 the volume V_f^m of agglomerates containing not less than m vacancies of the SS lattice within one agglomerate ($m=1$, filled circles; $m=2$, 3, 4, 5, 6, lines with dots) is shown in comparison with the quantity $V_f - \Delta V$, calculated with $\Delta V = 0.0298$ cm^3/g (empty circles). The solid lines represent a linear fit to the V_f ($m=1$) data in the temperature range above T_g. The dashed line shows the linear extrapolation of the ($V_f - \Delta V$) data. The inset shows the fractional hole free volume $f \equiv h$ analyzed from PVT experiments (symbols), extrapolated using Eq. (2) (solid line), linearly extrapolated (dashed line), and the expected behavior for the glass (dotted line).

Ortho-Ps responds to the holes size via collisions with the hole walls, which lead to its annihilation via the pickoff process. In case of elongated holes the collisions are less frequent in the direction of the long axes compared with the short axis. The nonlinear dependency of the *o*-Ps lifetime on the length of the hole axis [Eq. (3)] leads to its decreasing sensitivity to the long axis. When the Tao-Eldrup equation [32,33], which assumes spheres, is used for the calculation of the mean hole size, the calculated volume underestimates the true hole volume. In this case an equation equivalent to Eq. (3) but assuming cylindrical or cuboidal holes [41,42] may be applied. Since we only get the *o*-Ps lifetime τ_3 from experiments, the ratio of axis lengths has to be assumed in this kind of analysis. In the limiting case of very long tube-like holes, the lifetime mirrors mainly the diameter of the tube and cylindrical or rodlike holes of infinite length are a good approximation for the true hole shape.

For getting an impression of the magnitude of this effect we make some easy estimations. For simplicity we assume that the holes have a cuboid shape (rectangular parallelepiped). In this case the *o*-Ps lifetime follows the formula [41]

$$\lambda_{\rm po} = 1/\tau_{\rm po} = 2ns^{-1}\left\{1 - \prod_{i=1}^{3}\left[\frac{a_i}{a_i + 2\delta r} + \frac{1}{\pi}\sin\left(\frac{\pi a_i}{a_i + 2\delta r}\right)\right]\right\}, \tag{6}$$

where a_i are the cuboid side lengths and again $\delta r = 1.66$ Å. Assuming, for example, an experimental *o*-Ps lifetime of $\tau_3 = 2.0$ ns coming from a cuboidal hole with a length of twice the short axis $a_1 = a_2 = a_3/2 = a_h$, then the hole has as the size of $a_h = 4.40$ Å and a volume of $\nu_h = 170.4$ Å^3. When a cube hole shape is assumed in the calculation $a_1 = a_2 = a_3 = a_h$, this lifetime leads to a calculated size of $a = 5.16$ Å and a volume of $\nu_h = 137.4$ Å^3. For a specific free volume of $V_f = 0.10$ cm^3/g the true specific hole number for the cuboid is $N_h' = 0.1/170.4$ (cm^3/g)/Å$^3 = 0.59 \times 10^{21}$ g^{-1}. When applying the cube model, a hole number of $N_h' = 0.1/137.4$ (cm^3/g)/Å$^3 = 0.73 \times 10^{21}$ g^{-1} would be calculated. In case of very expanded holes, for example $a_3/5 = a_1 = a_2 = a_h = 2.07$ Å (resulting in $\tau_3 = 2.0$ ns), the cube model would underestimate the hole volume by a factor of 2.6. This leads to an overestimation of the hole density by the same factor. This shows that the hole density estimated from $N_h' = V_f/\langle \nu_h \rangle$ is an apparent value, which leads to the given value of V_f when being multiplied with the mean hole size calculated from τ_3 under the assumption of a certain shape of holes.

The discussed problem is not unknown in the literature. Schmidtke *et al.* [43] showed that in polymers holes have a cigarlike rather than a spherical shape. Hofmann *et al.* [37] have discussed a method of how to dissect complex holes found in computer simulations into simpler, more three-dimensional portions in order to simulate how *o*-Ps probes the free volume of an amorphous structure. From differences in the thermal expansion between the SS hole fraction h and

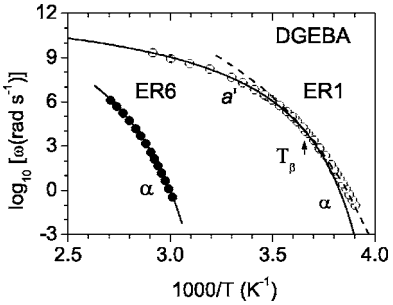

FIG. 9. Relaxation map of DGEBA-ER6 and DGEBA-ER1 showing the frequency ω of the primary dielectric relaxation process. The data were redrawn from Paluch *et al.* [19], Fig. 6, and Corezzi *et al.* [21], Fig. 7. The lines are fits of Eq. (7) to the data from the given range of temperatures.

o-Ps hole volume, Consolati *et al.* [18] concluded that the holes grow only in two dimensions. The nonspherical shape and the decreased sensitivity of the *o*-Ps probe to the long axis of a hole may cause a part of this effect. Summing up the discussion, it is clear that the *o*-Ps probe detects elongated holes as smaller ones but with a larger number when applying the formula for spheres or cubes in the calculation of the hole volume from τ_3.

The observed behavior of the hole sizes of ER1 and ER6 may be interpreted in terms of this picture in the following way: Imaging elongated holes, the *o*-Ps lifetime is strongly determined by the short axes of the holes. In the glassy state these axes mirror the intermolecular potential and forces, which are the same in ER1 and ER6. Therefore, the *o*-Ps lifetimes are almost the same. Owing to the longer molecular chains in ER6 the holes may be more elongated than in ER1. This causes the higher total free volume in the glassy state evidenced by its fraction h and specific volume V_f and the higher calculated (apparent) hole density N_h'. On the other hand ER1 needs a lower thermal energy for devitrification due to its lower molecular mass. This leads to the lower T_g and, at a given temperature, to higher frequencies and amplitudes of structural relaxation than in the case of ER6 (see Fig. 9). The increased structural relaxation and free volume fluctuation above T_g are mirrored in PALS as higher mean $\langle \nu_h \rangle$, and mean dispersion σ_h of hole volumes (Fig. 6), respectively.

C. Free volume and structural relaxation

As already mentioned, Paluch *et al.* [19] have published a detailed study of the dynamics of ER6. In this section we analyze the structural relaxation, as shown by dielectric spectroscopy in this work in terms of the free-volume model. As a starting point for the discussion, the relaxation map for ER6 [19] and ER1 [1,21] is shown in Fig. 9, i.e., Arrhenius plots of the characteristic circular frequencies $\omega = 1/\tau_{\max}$ of maximum in the dielectric loss ε'' of the primary process. Paluch *et al.* [19] have analyzed the data in terms of the Avramov equation [44]. For comparison with the results for ER1 we have reanalyzed the data of ER6 employing the conventional Vogel-Fulcher-Tammann (VTF) equation [45–47],

TABLE III. Parameters of the structural relaxation. The parameters come from the analysis of dielectric relaxation data from the temperature range between 332 and 369 K (ER6), and $T_\beta = 285$ K and 351 K (ER1, see Refs. [1,19]).

Quantity	Uncertainty	ER1	ER6
T_0 (K)	±1	234	286
B (K)	±60	720	1570
$\log_{10}\omega$ (rad s^{-1})	±0.7	14.8	14.3
ΔV (cm^3/g)	±0.001	0.0151	0.0298
γV_f^* (cm^3/g)	±0.03	0.445	0.819
$\log_{10} C$ (rad s^{-1})	±0.7	14.8	14.3
n	±0.3	1.5	2.2
$n\nu_{SS}$ (Å^3)	±10	57	100

$$\log_{10}\omega = \log_{10}\omega_0 - (B/\ln 10)/(T - T_0), \tag{7}$$

where T_0 is the temperature where the relaxation frequency approaches zero and B and ω_0 are constants. Including all data shown for ER6 in Fig. 9, the least-squares fit gives $T_0 = 286(\pm 3)$, $B = 1570(\pm 60)$ K, and $\log \omega_0 = 14.3(\pm 0.3)$ ($r^2 = 0.9999$) (Table III). The Vogel temperature T_0 is distinctly higher than the temperature where the (extrapolated) free volume vanishes, $T_0' = 223-233$ K (Tables I and II). This shows that the structural relaxation slows down faster than the shrinkage of the hole free volume V_f would predict on the basis of the free-volume theory.

The relaxation data of ER1 have been analyzed assuming different VTF behavior in different temperature ranges [1,21]. For the lower temperature range between $T_g = 255$ K and $T_\beta = 285$ K (the onset of the secondary β relaxation [21]) the fit provided $T_0 = 209 \pm 2$ K, $B = 2060 \pm 180$ K, and $\log_{10}\omega_0 = 18.0 \pm 0.7$. This T_0 agrees with the T_0' of ER1 (Tables I and II) with the consequence that the low-temperature relaxation follows the free-volume model. From the dielectric relaxation data of the temperature range between 285 and 351 K (denoted as the a' process [21]) the parameters $T_0 = 234.4 \pm 0.8$ K, $B = 720 \pm 20$ K, and $\log \omega_0 = 14.78 \pm 0.09$ were determined. For this temperature range $T_0 > T_0'$ as for ER6.

A difference between T_0 and T_0' causes a curvature in plots of $\log_{10}\omega$ vs the reciprocal specific free volume $1/V_f$, which can be observed in Fig. 10. The behavior indicates that the relaxation does not follow the Cohen-Turnbull relation $\log_{10}\omega = \log_{10} C - (\gamma V_f^*/\ln 10)/V_f$ [8] with V_f as calculated from the SS EOS. In this case the constants should be related, assuming that V_f follows Eq. (1), to those of the VFT law as $C = \omega_0$, $\gamma V_f^*/E_f = B$, and $T_0' = T_0$. γV_f^* is the minimum specific free volume required for the occurrence of the process, and $\gamma = 0.5-1$.

Following Utracki's approach for the viscosity [48] and our previous works [1,49] we linearize the dependency by substituting $1/V_f$ by $1/(V_f - \Delta V)$ with a suitable chosen value of ΔV,

$$\log_{10}\omega = \log_{10} C - (\gamma V_f^*/\ln 10)/(V_f - \Delta V). \tag{8}$$

The fit of Eq. (8) to the data of ER6 shown in Fig. 10 delivers the parameters $\gamma V_f^* = 0.819(\pm 0.03)$ cm^3/g, ΔV

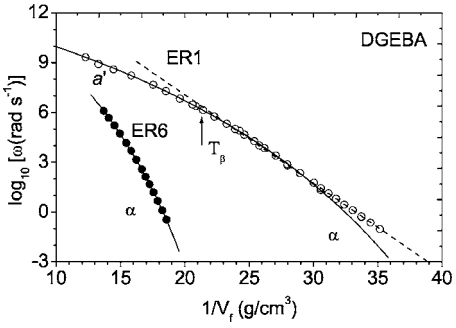

FIG. 10. "Modified" relaxation map (Cohen-Turnbull plot) of the primary dielectric relaxation process. The lines are fits of Eq. (8) to the experimental data, for DGEBA-ER6 in the temperature range from 330 to 370 K (ΔV=0.0298 cm^3/g) and for DGEBA-ER1 in the temperature range from 285 to 350 K (a' process, ΔV =0.015 cm^3/g) and from 255 to 285 K (α process, ΔV=0).

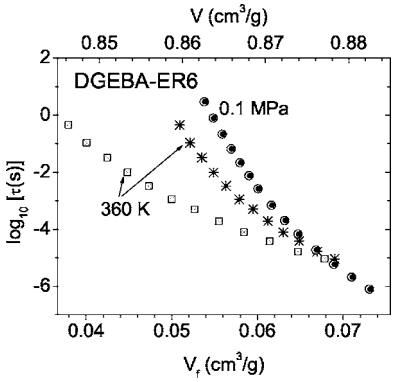

FIG. 11. Comparison of isothermal (crosses and cross-centered squares) and isobaric (open and filled circles) dependencies of relaxation times $\tau=1/\omega$ (from Ref. [19]) plotted as a function of the free volume $V_f(T,P)$ (bottom x axis, crosses and open circles) and of the total volume $V(T,P)$ (top x axis, cross-centered squares and filled circles) for DGEBA-ER6. The V_f and V axis were scaled so that the first and the last data point of the isobaric data match.

=0.0298(±0.001) cm^3/g, and $\log_{10} C$=14.3(±0.3) (r^2 =0.9999). The value of ΔV corresponds to the difference $E_{f0}(T_0-T_0')$=0.031 cm^3/g. In case of ER1 the fit in the temperature range above T_β gives γV_f^*=0.445(±0.001) cm^3/g, ΔV=0.0151±0.001 cm^3/g, and $\log_{10} C$=14.8±0.1 (Table III).

Our results show that it is not the entire hole free volume V_f that is related to the structural relaxation via the Cohen-Turnbull free-volume theory but rather it is a smaller portion, $V_f-\Delta V$. As discussed in our previous works [1,49] we may understand this behavior when assuming that monovacancies in the SS lattice present too small a local free volume to show a liquidlike behavior. Multivacancies may, however, show this behavior. For estimation of their size we have calculated that part of the specific free volume V_f^m, which appears in the form of multivacancies and contains m or more vacancies (unoccupied cells of the SS lattice). The calculation uses results of Monte Carlo simulations by Vleeshouwers *et al.* [11] and is described in detail in Ref. [1].

The partial volumes V_f^m of ER6 for $m=1,\ldots,6$ are shown in Fig. 8. For ER6 we also plotted the value $V_f-\Delta V$ (ΔV =0.0298 cm^3/g), which is the part of the free volume that controls the structural relaxation via the Cohen-Turnbull relation. From a comparison of $(V_f-\Delta V)$ with V_f^m it follows that to allow the structural relaxation in ER6 a multivacancy must have a minimum size corresponding, on average, to n $\approx$2.2 of the volume of the SS lattice cell, that is, $n\times\nu_{SS}$ $\approx$100 Å^3 (ν_{SS}=45 Å^3). For ER1 [1] we estimated $n\approx1.5$ corresponding to $n\times\nu_{SS}\approx$57 Å^3 (ν_{SS}=38.3 Å^3, Table I). For the polymer polyvinylacetate some of us got $n\approx3$ corresponding to $n\times\nu_{SS}\approx$138 Å^3 (ν_{SS}=46 Å^3) [49]. These values show that with increasing molecular chain length the minimum hole (vacancy agglomerate) size required to describe the structural relaxation process via the free volume model increases systematically. On the other hand, it is well known that the transport of small molecules through polymers usually can be described by the Cohen-Turnbull free volume theory when estimating the free volume either from PVT (SS EOS) [50] or PALS [51,52] experiments.

Finally, we remark that Eq. (2), which describes the equilibrium concentration of vacancies in the SS lattice, opens a different way for an extrapolation of the equilibrium part of the free volume into the glassy state, which goes beyond the simple linear extrapolation. To illustrate this point, the inset in Fig. 8 shows the fractional hole free volume $f\equiv h$ analyzed from the PVT experiments via the SS EOS and the linear extrapolation as well as the extrapolation employing Eq. (2). As can be observed, the extrapolated f from Eq. (2) decreases gradually and becomes zero only when 0 K is reached. It has a value of 0.01 at T_0'=223 K and of 0.0001 at 130 K. Assuming that the structural relaxation is governed by the equilibrium part of the free volume given by Eq. (2) this behavior seems to be irreconcilable with the current manner of fitting the VFT equation to the relaxation-time data of supercooled liquids. The variation of f formally does not lead to a singularity in the relaxation time τ at a temperature above the absolute zero. The linear fit to f (or V_f), which leads to the VFT equation appears now as an approximation. As the figure shows, for ER6 the linear fit is, however, a good approximation up to temperatures of ~260 K, that is, 65 K below T_g.

We remark that some years ago Johari [53] had proposed an interpolation scheme for the equilibrium heat capacity C_p assuming a sigmoid-shape change over a broad temperature range from above T_g to 0 K. This behavior of C_p does not show the discontinuity in C_p at the Kauzmann [54] temperature T_k. Future research may enlighten these interesting problems.

Next we discuss the pressure dependency of relaxation times. From a Cohen-Turnbull fit to the dielectric relaxation data of Paluch *et al.* [19] recorded at 360 K in the pressure range between 0.1 and 110 MPa (not shown) we obtained the volume parameter ΔV=0.031(±0.003) cm^3/g, which corresponds to the estimate from the 0.1 MPa isobar.

In Fig. 11 we show plots of isobaric (at 0.1 MPa) and isothermal (at 360 K) relaxation times, $\tau(T,P)=1/\omega(T,P)$ (from Paluch *et al.* [19], Fig. 6) vs the free volume $V_f(T,P)$ and the same plots vs the total volume $V(T,P)$. The isobaric data agree perfectly over the whole range of volumes (tem-

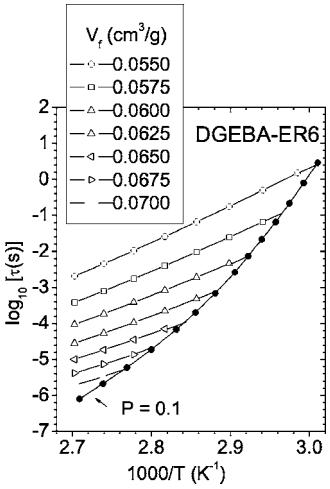

FIG. 12. Isochoric relaxation times (empty symbols) at the indicated specific free volumes V_f, along with the relaxation times for ambient pressure (filled circles) for DGEBA-ER6. The relaxation data are from Ref. [19].

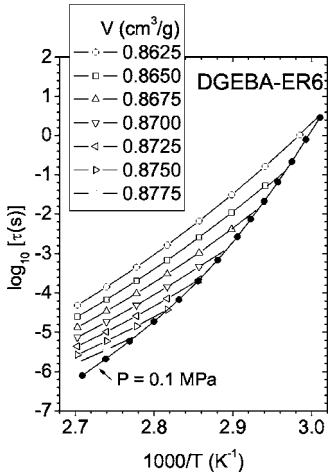

FIG. 13. Isochoric relaxation times (empty symbols) at the indicated specific total volumes V, along with the relaxation times for ambient pressure (filled circles) for DGEBA-ER6. The relaxation data are from Ref. [19].

peratures). The reason for this behavior is that V_{occ} is nearly constant (above T_g) and V changes almost exclusively due the variation in V_f.

The isothermal plots of $\log \tau$ vs V_f and vs V, however, clearly disagree since V contains the occupied volume V_{occ}, which is compressible. The discrepancy is highly reduced when plotting the data vs V_f. The remaining differences can be attributed to deviations from the free-volume model (such as $\Delta V \neq 0$ shows) and the role of temperature in the relaxation process. We mention that the pressure-dependent relaxation data of Corezzi *et al.* [55] for ER1 analyzed in our preceding work [1] show a corresponding behavior.

D. Role of volume and temperature in the structural dynamics

In the literature there are several attempts to include simultaneously the effect of thermal energy and volume in the analysis of structural dynamics of glass-forming liquids and to quantify the degree to which both quantities govern the dynamics, without assuming a certain model for dynamics. The usual approach is to determine the ratio of the (apparent) activation enthalpies $E_i = R\,[(d \ln \tau / dT^{-1})]_i$ at constant volume V and constant pressure P [19,22–27],

$$E_V/E_P = [(d \log_{10} \tau/dT^{-1})]_V/[(d \log_{10} \tau/dT^{-1})]_P, \qquad (9)$$

where τ is again the relaxation time of structural relaxation. The ratio E_V/E_P, equal to the ratio of the corresponding isochoric and isobaric fragilities, can vary from 0 (corresponding to volume-dominated dynamics) to unity (temperature as the control variable) and has been found to fall at temperatures near T_g in the range from 0.38 to 0.64 in case of molecular liquids and from 0.52 to 0.81 for polymers. From this value it has been concluded that the change in structural relaxation time upon cooling toward the glass transition is due to both thermal contraction of the material and its energy loss, the latter exerting a somewhat stronger effect in most polymers ($E_V/E_P > 0.5$) with the exception of polyphenylene oxide ($E_V/E_P = 0.25$), which was attributed to its flexible chain structure [25–27]. The underlying idea is that structural motions are thermally activated but impeded by steric constraints (jamming); this confers a volume dependence to the activation enthalpy and leads to the non-Arrhenius behavior ($\log \tau$ not proportional to T^{-1}).

We criticize the use of enthalpy at constant total volume E_V in the enthalpy ratio with the following arguments. (i) The total volume is not the controlling volume parameter of structural relaxation but the hole (or excess) free volume is. (The occupied volume is related to vibrations and not to segmental relaxations.) (ii) The hole free volume $V_f(T,P)$ is not the same for the same total volume $V(T,P)$ but different T, P pairs. Recently, some of us [50] have shown that arguments against the validity of the free-volume theory for describing the electrical conductivity of polymer electrolytes [56] vanish when assuming that V_f (and not V) is the controlling volume parameter.

Considering these arguments we suggest the employment of the activation enthalpy at constant specific (hole) free volume,

$$E_{Vf} = R[(d \ln \tau/dT^{-1})]_{Vf}, \qquad (10)$$

which modifies Eq. (9) to

$$E_{Vf}/E_P = [(d \log_{10} \tau/dT^{-1})]_{Vf}/[(d \log_{10} \tau/dT^{-1})]_P. \qquad (11)$$

In Fig. 12 we have shown Arrhenius plots of the isobaric, $[\tau(T)]_P$ ($P = 0.1$ MPa), and isochoric, $[\tau(T)]_{Vf}$ ($V_f = 0.055\ \mathrm{cm}^3/\mathrm{g}, \ldots, 0.0700\ \mathrm{cm}^3/\mathrm{g}$), relaxation times of ER6. To determine the isochoric data, we have first calculated for temperatures T in the range between 330 and 375 K in steps of 5 K and a fixed free volume V_f the corresponding pressures P from Eq. (1). Then, for a given T, P pair the relaxation time τ was calculated using the Avramov equation [44] with the parameters given for dielectric relaxation in DGEBA-ER6 by Paluch *et al.* [19].

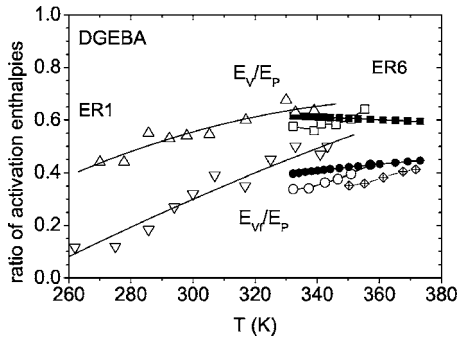

FIG. 14. Ratio of activation enthalpies at constant total, E_V/E_P, or free, E_{Vf}/E_P, volume to the enthalpy at constant pressure calculated from Eq. (9) (E_V/E_P, empty squares—ER6 and up-triangles—ER1) and Eq. (11) (E_{Vf}/E_P, empty circles—ER6 and down-triangles—ER1, all for $P=0.1$ MPa). The cross-centered diamonds show E_{Vf}/E_P for ER6 and $P=50$ MPa. Filled symbols show corresponding ratios calculated from Eq. (12) (E_V/E_P, squares) and Eq. (13) (E_{Vf}/E_P, circles) for ER6 and $P=0.1$ MPa. The lines are a guide for the eyes.

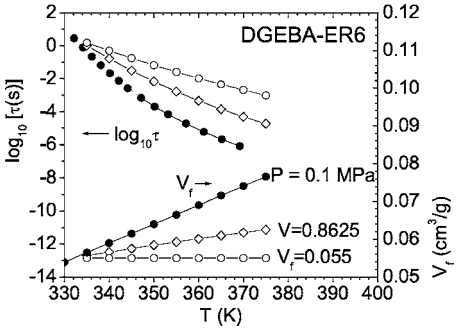

FIG. 15. Relaxation times τ of segmental relaxation for constant free ($V_f=0.055$, empty circles) and total ($V=0.8625$, empty diamonds) volume along with the relaxation times for ambient pressure (filled circles) and the corresponding specific free volumes V_f as a function of temperature T for DGEBA-ER6.

The isobars are the experimental data of these authors for $P=0.1$ MPa. The slopes at the intersection of the isochoric and isobaric curves yield the respective activation enthalpies for ambient pressure. For comparison, Fig. 13 shows the traditional plots of the relaxation time at constant total volume, $[\tau(T)]_V$ ($V=0.8625$ cm$^3/g,\ldots,0.8775$ cm^3/g). Here we have calculated P for given T and V from the Tait equation [28] least squares fitted to our volume data.

Figure 14 displays the enthalpy ratios at $P=0.1$ MPa for ER6 and also for ER1. The latter were calculated (not shown) using our previous volume data [1] and the relaxation times published by Corezzi *et al.* [21,55]. Tentatively we have also calculated E_P for ER6 at $P=50$ MPa and shown in Fig. 14 the corresponding ratio E_{Vf}/E_P. Generally, both values E_V/E_P and E_{Vf}/E_P change as expected: they increase with increasing free volume, i.e., with increasing temperature, decreasing pressure, and decreasing molecular weight of the DGEBA molecules.

The comparison of Figs. 12 and 13 shows that the plots at constant V_f are less steep than those at constant V. This leads to smaller values of E_{Vf}/E_P than of E_V/E_P and to the general inference that the free volume plays a larger role in dynamics than concluded from the ratio E_V/E_P. The reason for the too-large values of E_V/E_P is illustrated in Fig. 15. The assumed constancy of the total volume V requires an increasing pressure with increasing temperature. Since the free volume $V_f(T,P)$ increases with increasing P [for fixed $V(T,P)$] the relaxation times are smaller compared with the values for constant V_f. Or, in other words, to hold V constant with increasing temperature requires a smaller pressure than when holding V_f constant, and leads therefore to a shorter relaxation time at a given temperature.

Another approach to quantify the degree to which thermal energy and density govern the dynamics is the scaling of relaxation times by expressing them as a function of temperature and volume [25–27]. It is found that structural relaxation times τ for several glass-forming liquids and polymers, measured as isotherms at varying pressures and as isobars at varying temperatures, superpose when plotted vs $T^{-1}V^{-\gamma}$, where γ is a suitable chosen material-specific constant. The underlying idea is that the repulsive part of the potential dominates the local liquid structure and follows an inverse power law $\varphi(r)\propto r^{-3\gamma}$. Thus, $\gamma=4$ is expected for a Lennard-Jones potential. It was shown that the ratio $[E_V/E_P]_T$ can be expressed by

$$[E_V/E_P]_T=[1+\gamma T\alpha_P(T)]^{-1}, \tag{12}$$

where $\alpha_P(T)=\alpha_r(T)$ is the isobaric thermal expansion coefficient of the total volume [25–27].

We have performed such scaling and show it for ER6 in Fig. 16 (bottom part). A value of $\gamma=3.0(\pm0.2)$ is found, which corresponds to the ratio $[E_V/E_P]_T=0.62-0.60$ for $P=0.1$ MPa (Fig. 14). These values have the same magnitude as those estimated from Eq. (9) (Fig. 14); they decrease, however, with increasing temperature [27].

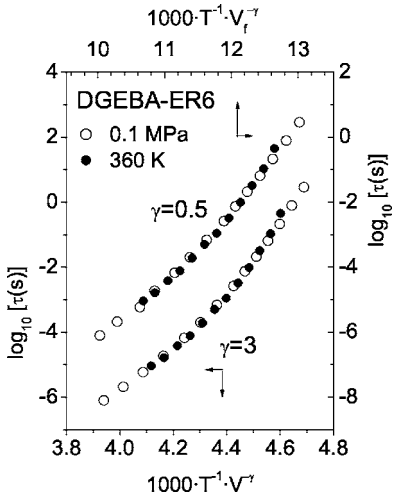

FIG. 16. Specific-volume-scaled Arrhenius plots of isobaric (open circles) and isothermal (filled circles) dielectric relaxation times τ for DGEBA-ER6. Bottom plot: total-volume scaling ($\gamma=3.0$), top plot: free-volume scaling ($\gamma=0.5$). The experimental relaxation times are from Ref. [19].

We have attempted to scale the relaxation times by the free volume V_f and found that plots of isotherms and isobars vs $T^{-1}V_f^{-\gamma}$ superpose for $\gamma=0.5(\pm 0.1)$ (see Fig. 16, top part). While γ of Eq. (12) is related to the exponent of the repulsive potential, the physical meaning of this value of γ is not yet clear to us. We can, however, derive a relation like Eq. (12) for the free volume using our definition of E_{Vf} in Eq. (10) and following the line of the derivation for the total volume. We obtain the relation

$$[E_{Vf}/E_P]_T=[1+\gamma T\alpha_{fP}(T)]^{-1}, \tag{13}$$

where $\alpha_{fP}(T)=\alpha_{f,r}(T)$ is the isobaric thermal expansion coefficient of the free volume and γ is now the scaling exponent with respect to the free volume. The values of $[E_{Vf}/E_P]_T$ calculated from this relation for $P=0.1$ MPa are also shown in Fig. 14.

Recently, the decrease of $[E_V/E_P]_T$ estimated from Eq. (12) with increasing temperatures observed for several low molecular glass-forming liquids was interpreted as being at odds with free-volume interpretation of the glass transition [27]. One can observe, however, in Fig. 14 that, unlike $[E_V/E_P]_T$, the quantity $[E_{Vf}/E_P]_T$ shows the expected increase.

The reason for this different behavior is the following. When the free volume follows Eq. (1), $V_f=E_f(T-T_0')$, then $T\alpha_{fP}=T/(T-T_0')$ always decreases with increasing temperature. This value is independent of the pressure or may increase when T_0' increases with P. T_0' is smaller in the low than in the high molecular weight DGEBA (Table I), which leads to a lower value of $T\alpha_{fP}$. The behavior of $T\alpha_{fP}$ causes a variation of $[E_{Vf}/E_P]_T$, which is in complete agreement with the expectation from the free-volume theory: the enthalpy ratio increases with increasing free volume, i.e., with increasing temperature, decreasing pressure, and decreasing molecular weight of the molecule. The latter effect depends strongly, however, on the value of γ.

For the total volume $V(T,P)=V_{\mathrm{occ}}(T,P)+V_f$ $(T,P)=V_{\mathrm{occ}}(T,P)+E_{f0}(P)$ $(T-T_0')$, one gets $T\alpha_P=E_{f0}(P)$ $(T-T_0')/[V_{\mathrm{occ}}(P)+E_{f0}(P)(T-T_0')]$. This value decreases with increasing temperature only if $V_{\mathrm{occ}}(T,P)<E_{f0}(P)T_0'$. We have, however, typically $V_{\mathrm{occ}}=0.5-1$ cm^3/g and $E_{f0}T_0'=0.1-0.3$ cm^3/g and therefore $\partial(T\alpha_P)/\partial T>0$. This causes $T\alpha_P$ to increase and $[E_V/E_P]_T$ to decrease with increasing temperature which is, as concluded previously [27], at odds with the expectation. Future research may bring further progress in understanding these interesting relations.

IV. CONCLUSIONS

The oligomeric epoxy resin of DGEBA (ER6) shows systematic differences to the monomeric liquid of the same resin (ER1) in free volume and structural relaxation. These differences are mirrored in the molecular mass of the MER of the SS lattice determined from the SS EOS: the MER of ER6 is more heavy and bulky and the chain less flexible than that of ER1. ER6 shows in the glassy state the same mean o-Ps lifetime and therefore the same mean apparent hole sizes as ER1 but a higher specific free volume V_f and hole density N_h'. This behavior is explained by assuming elongated holes of the same diameter (due to the same intermolecular potential and forces) but more elongated in the oligomer than in the monomer. In the liquid, the volume parameters V_f and $\langle\nu_h\rangle$ (due to the higher T_g) and also dV_f/dT and dV_f/dP (due to the less flexible chain) are smaller for ER6.

The reported dielectric α-relaxation time τ shows certain deviations from the Cohen-Turnbull free-volume model that are larger for ER6 than for ER1. Plots of the relaxation frequency $\log_{10}\omega$ vs the $1/V_f$ show a curved dependency, which can be linearized assuming that $\log_{10}\omega$ follows the function $1/(V_f-\Delta V)$. The fits deliver $\Delta V=0.0298$ cm^3/g for ER6 and $\Delta V=0.015$ cm^3/g for ER1. This behavior was explained by the picture that monovacancies in the SS lattice present too small a local free volume to show a liquidlike behavior, but multivacancies may show this behavior. Their minimum size was determined to $n\approx 2.2$ for ER6 and $n\approx 1.5$ for ER1 in units of the SS cell size.

Like in polymers, the hole free-volume fraction h in the liquid follows the Schottky equation $h\propto\exp(-H_h/k_BT)$, where H_h corresponds to $\sim 1/3$ of the cohesive energy of the SS MER. This behavior allows one to extrapolate the equilibrium part of the free volume without assuming a linear dependency. h decreases gradually with decreasing slope below T_g and becomes formally zero only when 0 K is reached. This behavior means that no singularity would appear in the relaxation time at temperatures above 0 K.

The degree to which volume and thermal energy govern the structural dynamics is frequently attempted to quantify by the ratio of the activation enthalpies at constant volume V and at constant pressure P, E_V/E_P. We argued that the free volume $V_f(T,P)$ and not the total volume $V(T,P)$ is the volume parameter that controls the dynamics and showed that $V_f(T,P)$ is not the same for the same $V(T,P)$ but different T,P pairs. Therefore, we suggested substituting E_V by E_{Vf}, the activation enthalpy at constant hole (or excess) free volume. E_{Vf}/E_P changes as expected: it increases with increasing free volume, i.e., with increasing temperature, decreasing pressure, and decreasing molecular weight. E_{Vf}/E_P exhibits smaller values than E_V/E_P, which shows that the free volume plays a larger role in structural dynamics than concluded from E_V/E_P. The same conclusion is obtained when scaling τ to $T^{-1}V_f^{-\gamma}$instead of to $T^{-1}V^{-\gamma}$ where both γ's are material constants.

ACKNOWLEDGMENTS

We thank M. Paluch (Katowice) for supplying the numerical data of dielectric relaxation measurements and for stimulating comments to the subject. J. Kansy (Katowice) is acknowledged for delivering the new routine LT9.0 and D. Kilburn (Bristol) for a critical reading of the manuscript. One of us (E.M.H.) wishes to thank the Deutscher Akademischer Austauschdienst and the Martin-Luther-University Halle-Wittenberg for support.

[1] G. Dlubek, E. M. Hassan, R. Krause-Rehberg, and J. Pionteck, Phys. Rev. E **73**, 031803 (2006).
[2] R. Simha and T. Somcynsky, Macromolecules **2**, 342 (1969).
[3] R. E. Robertson, in *Computational Modelling of Polymers*, edited by J. Bicerano (Marcel Dekker, Midland, MI, 1992), p. 297.
[4] L. A. Utracki and R. Simha, Macromol. Theory Simul. **10**, 17 (2001).
[5] D. Porter, *Group Interaction Modelling of Polymer Properties* (Marcel Dekker, Inc., New York, 1995), p. 87.
[6] A. K. Doolittle, J. Appl. Phys. **22**, 1471 (1951).
[7] A. Bondi, J. Phys. Chem. **68**, 441 (1964); A. Bondi, *Physical Properties of Molecular Crystals, Liquids, and Gases* (Wiley, New York, 1968), p. 450.
[8] M. H. Cohen and D. Turnbull, J. Chem. Phys. **31**, 1164 (1959); D. Turnbull and M. H. Cohen, *ibid.* **52**, 3038 (1970).
[9] O. E. Mogensen, *Positron Annihilation in Chemistry* (Springer, Berlin, Heidelberg, 1995).
[10] *Principles and Application of Positron and Positronium Chemistry*, edited by Y. C. Jean, P. E. Mallon, and D. M. Schrader (World Scientific, Singapore, 2003).
[11] S. Vleeshouwers, J.-E. Kluin, J. D. McGervey, A. M. Jamieson, and R. Simha, J. Polym. Sci., Part B: Polym. Phys. **30**, 1429 (1992).
[12] G. Dlubek, J. Pionteck, and D. Kilburn, Macromol. Chem. Phys. **205**, 500 (2004); G. Dlubek, V. Bondarenko, I. Y. Al-Qaradawi, D. Kilburn, and R. Krause-Rehberg, *ibid.* **205**, 512 (2004).
[13] G. Dlubek, A. SenGupta, J. Pionteck, R. Krause-Rehberg, H. Kaspar, and K. H. Lochhaas, Macromolecules **37**, 6606 (2004); G. Dlubek, J. Wawryszczuk, J. Pionteck, T. Goworek, H. Kaspar, and K. H. Lochhaas, Macromolecules **38**, 429 (2005).
[14] D. Kilburn, G. Dlubek, J. Pionteck, D. Bamford, and M. A. Alam, Polymer **46**, 559 (2005).
[15] G. Dlubek, J. Non-Cryst. Solids **352**, 2869 (2006).
[16] R. Srithawatpong, Z. L. Peng, B. G. Olson, A. M. Jamieson, R. Simha, J. D. McGervey, T. R. Maier, A. F. Halasa, and H. Ishida, J. Polym. Sci., Part B: Polym. Phys. **37**, 2754 (1999).
[17] M. Schmidt and F. H.-J. Maurer, Macromolecules **33**, 3879 (2000).
[18] G. Consolati, J. Phys. Chem. B **109**, 10096 (2005); G. Consolati, F. Quasso, T. Simha, and B. G. Olson, J. Polym. Sci., Part B: Polym. Phys. **43**, 2225 (2005).
[19] M. Paluch, C. M. Roland, J. Gapinski, and A. Patkowski, J. Chem. Phys. **118**, 3177 (2003).
[20] T. Koike, Adv. Polym. Sci. **149**, 140 (1999).
[21] S. Corezzi, M. Beiner, H. Huth, K. Schröter, S. Capaccioli, R. Casalini, D. Fioretto, and E. Donth, J. Chem. Phys. **117**, 2435 (2002).
[22] G. Williams, in *Dielectric Spectroscopy of Polymeric Materials*, edited by J. P. Runt and J. P. Fitzgerald (American Chemical Society, Washington, D.C., 1997).
[23] M. Paluch, R. Casalini, and C. M. Roland, Phys. Rev. B **66**, 092202 (2002).
[24] C. M. Roland, M. Paluch, T. Pakula, and R. Casalini, Philos. Mag. **84**, 1573 (2004).
[25] C. M. Roland, S. Hensel-Bielowka, M. Paluch, and R. Casalini, Rep. Prog. Phys. **68**, 1405 (2005).
[26] C. M. Roland and R. Casalini, J. Non-Cryst. Solids **351**, 2581 (2005).
[27] C. M. Roland, K. J. McGrath, and R. Casalini, e-print cond-mat/0601388.
[28] P. Zoller and C. J. Walsh, *Standard Pressure-Volume-Temperature Data for Polymers* (Technomic Publishing Co., Inc., Lancaster, Basel, 1995).
[29] W. Schottky, Phys. Z. **23**, 448 (1922).
[30] J. Perez, *Physics and Mechanics of Amorphous Polymers* (A. A. Balkema, Rotterdam, Brookfield, 1998), p. 18.
[31] J. Kansy, Nucl. Instrum. Methods Phys. Res. A **374**, 235 (1996); J. Kansy (private communication).
[32] S. J. Tao, J. Chem. Phys. **56**, 5499 (1972).
[33] M. Eldrup, D. Lightbody, and J. N. Sherwood, Chem. Phys. **63**, 51 (1981).
[34] N. Nakahishi and Y. C. Jean, in *Positron and Positronium Chemistry, Studies in Physical and Theoretical Chemistry*, edited by D. M. Schrader and Y. C. Jean (Elsevier Science Publishers, Amsterdam, 1988), Vol. 57, p. 159.
[35] R. B. Gregory, J. Appl. Phys. **70**, 4665 (1991).
[36] J. Liu, Q. Deng, and Y. C. Jean, Macromolecules **26**, 7149 (1993).
[37] D. Hofmann, M. Entrialgo-Castano, A. Lerbret, M. Heuchel, and Y. Yampolskii, Macromolecules **36**, 8528 (2003).
[38] M. Heuchel, D. Hofmann, and P. Pullumbi, Macromolecules **37**, 201 (2004).
[39] X.-Y. Wang, P. J. int Veld, Y. Lu, B. D. Freeman, and I. C. Sanchez, Polymer **46**, 9155 (2005).
[40] G. Dlubek, J. Stejny, and M. A. Alam, Macromolecules **31**, 4574 (1998).
[41] T. Goworek, K. Ciesielski, B. Jansińska, and J. Wawryszczuk, Chem. Phys. **230**, 305 (1998); B. Jasińska, A. E. Kozioł, and T. Goworek, *5th International Workshop on Positron and Positronium Chemistry (ppc 5)*, June 9–14, Lillafüred, Hungary, edited by Zs. Kajcsos, B. Lévay, and K. Süvegh [J. Radioanal. Nucl. Chem. **210**, 617 (1996)].
[42] T. L. Dull, W. E. Frieze, D. W. Gidley, J. N. Sun, and A. F. Yee, J. Phys. Chem. B **103**, 4657 (2001).
[43] E. Schmidtke, K. Günther-Schade, D. Hofmann, and F. Faupel, J. Mol. Graphics Modell. **22**, 309 (2004).
[44] I. Avramov, J. Non-Cryst. Solids **262**, 258 (2000).
[45] H. Vogel, Phys. Z. **22**, 645 (1921).
[46] G. S. Fulcher, J. Am. Ceram. Soc. **8**, 339 (1925).
[47] G. Tammann and W. Hesse, Z. Anorg. Allg. Chem. **156**, 245 (1926).
[48] L. A. Utracki, Polym. Eng. Sci. **25**, 655 (1985).
[49] G. Dlubek, D. Kilburn, and M. A. Alam, Macromol. Chem. Phys. **206**, 818 (2005).
[50] G. Dlubek, D. Kilburn, and M. A. Alam, Electrochim. Acta **49**, 5241 (2004); **50**, 2351 (2005).
[51] D. Bamford, A. Reiche, G. Dlubek, F. Alloin, J.-Y. Sanchez, and M. A. Alam, J. Chem. Phys. **118**, 9420 (2003).
[52] C. Nagel, K. Günther- Schade, D. Fritsch, T. Strunskus, and F. Faupel, Macromolecules **35**, 2071 (2002).
[53] G. P. Johari, J. Chem. Phys. **113**, 751 (2000).

[54] W. Kauzmann, Chem. Rev. (Washington, D.C.) **43**, 219 (1948).

[55] S. Corezzi, P. A. Rolla, M. Paluch, J. Ziolo, and D. Fioretto, Phys. Rev. E **60**, 4444 (1999); S. Corezzi, S. Capaccioli, R. Casalini, D. Fioretto, M. Paluch, and P. A. Rolla, Chem. Phys. Lett. **320**, 113 (2000).

[56] J. T. Bendler, J. J. Fondanella, M. F. Shlesinger, and M. C. Wintersgill, Electrochim. Acta **48**, 2267 (2003).